

# Numerical simulation of intravenous blood flow

**Amir Haghhighatkha**  
Master of Mechanical Engineering  
Tehran, Iran  
haghhighatkha.eng@gmail.com

**Milad Abdollahi Kahriz**  
Tehran, Iran  
Miladmak@yahoo.com

**Abstract**—Many cardiovascular diseases that endanger human life and health are related to the conditions of blood flow inside the arteries. By simulating blood flow inside clogged arteries and examining the parameters affecting it, the complications and effects of this disease can be studied. The main purpose of this study is to analyze the effect of different parameters and clogs (25%, 50% and 75%) for pulsed blood flow within the viscoelastic artery. Progression of atherosclerosis causes an increase in elastic modulus and a 64% decrease in radial displacement of the arterial wall and an increase of 11 and 12% in the size and speed of blood flow. Increasing the value of the power index increases the maximum amount of shear stress of the wall at the site of clogging

**Keywords**— *Stiffness, Viscoelastic artery, Fluid-structure interaction, Non-Newtonian fluid.*

## I. INTRODUCTION

Cardiovascular diseases are one of the most common diseases in today's society. These diseases may affect the heart valves or arteries, especially the arteries. Arterial disease of the heart includes dilation of the arteries, closure of the arteries, or hardening of the arteries. When the arteries become narrow, they can no longer supply oxygen to the heart cells, endangering human life. One of the most common diseases in this field is thickening of the arterial walls. Thickening of the arterial wall leads to a decrease in the elasticity of the artery and as a result its clogging directly affects the hydrodynamic parameters of blood flow including changes in velocity and pressure inside the artery and mechanical behavior of the arterial wall. The presence of this obstruction leads to the formation of eddy areas, which in turn causes hypertension [1]. Smith [2] has studied the stable and incompressible blood flow using an analytical method. The results of his study show that the flow pattern is highly dependent on Reynolds flow clogging geometry. Deshpande et al. [3] simulated stable blood flow within an artery with axially symmetrical occlusion. Their results show that in moderate clogging and low Reynolds numbers, no separation zone is observed and only in the narrowing part (clogging region) the current is slightly unstable, but with increasing clogging intensity in high Reynolds numbers, the flow separation region in Young and Tsai [4] studied the stable flow of Newtonian blood fluid inside a hard-walled artery in the laboratory. They examined the types of cramps in axially symmetric conditions for a calm and turbulent flow regime. Their results show that increasing clogging and flow inertia can lead to the formation of strong and large vortices in the artery.

Johnston et al. [6,5] investigated the application of different rheological models to stable and transient currents within the rigid artery. Non-Newtonian models have the ability to predict the decrease in viscosity at high strain rates. Buchanan et al. [7] investigated the effects of rheological blood models on pulsed flow within rigid arteries with axial symmetry. Their results show that the selection of rheological models is very effective in changing the shear stress of the wall.

Hussain [8] simulated the flow of non-Newtonian blood fluid into a clogged rigid vessel using Comsol software. He examined the shear stress on the artery wall for different flow rates and clogging rates. His results show that the Newtonian model is a good approximation for wall shear stress at high strain rates and the generalized power law model is a better approximation for wall shear stress at low strain rates. Jung et al. [9] studied the flow of non-Newtonian fluids under rigid axial symmetric conditions with 45% clogging. They investigated the effects of clogging intensity and shear stresses by considering trapezoidal profiles for clogging modeling. They showed that increasing the severity of the blockage leads to an increase in shear stress of the wall at the site of the blockage. Using a numerical method, Perktold et al. [10] studied the effects of the expandable artery wall on the flow field and shear stresses of the wall and described vortex-shaped areas by considering blood flow in the arterial artery. Using the transient, incompressible, and three-dimensional shapes, they performed the Navier-Stokes equations for the non-Newtonian fluid and the linear shell theorem for the elastic wall. Zaušková et al. [11] numerically studied the non-Newtonian blood flow within symmetrical elastomeric arteries. By comparing Newtonian and non-Newtonian fluids, they examined the deformation and shear stress of the wall for a straight tube with a blockage. They found that the shear stress of the wall depended significantly on the geometry of the clogging, and that blood rheology would only affect the shear stress of the wall. Using the interaction of fluid and structure, Chan et al. [12] simulated the pulsating flow of blood inside a vessel with axially symmetrical occlusion. Using non-Newtonian and Newtonian fluids for blood and elastic and isotropic solids for the wall, they simulated the flow in Ansys and fultron software. Their results show that wall expansion reduces axial velocity and increases flow reversal effects. Cho et al. [13] Using fluid and structural interaction method, investigated the changes in blood vessels using Ansys and cfx software. In their study, non-Newtonian blood fluid inside the vessel with 50% clogging for modules Different elastics have been simulated. They found that the greater the elasticity of the blood vessel, the

larger the periods of velocity and pressure and the changes in shear stress and the smaller the length of the return flow region. Using turbulence models, Lee et al. [14] simulated the flow inside an elastic artery with varying degrees of occlusion. To simulate the flow, they used Fluent and Abacus software. Their results show that increasing the severity of the blockage leads to high pressure drop, increased blood velocity and peak shear stress of the wall in the clogging area.

In the present study, the effect of different vessel geometry (different rate of vessel occlusion) on the hydrodynamic parameters of non-Newtonian blood flow in the artery with viscoelastic wall was investigated. For this purpose, the interaction between the fluid and the structure at the point of contact of blood flow with the artery wall is considered.

## II. STATEMENT OF THE PROBLEM

A two-dimensional axial symmetric geometry is used to simulate the flow inside the artery, with a diameter of 4 mm without clogging and a total length of 276 mm. The schematic of the geometry is shown in Figure (1).

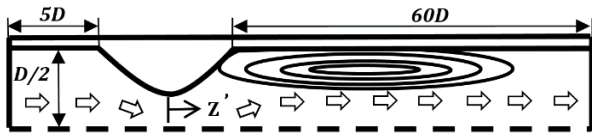


Figure 1. Schematic of clogged artery geometry

To validate the developed numerical model, the results are compared with Lee and Xu [15]. Blood flow simulation has also been done with the help of coding in COMSOL software. This software uses the finite element method to solve partial differential equations.

## III. EQUATIONS

Blood is considered as an incompressible, non-Newtonian and isothermal fluid and its flow is slow. Assuming incompressibility and zero gravitational force, the mass and momentum survival equations governing the flow of the problem are expressed as follows.

$$\nabla \cdot U_f = 0 \quad (1)$$

$$\rho_f \left[ \frac{\partial U_f}{\partial t} + (U_f \cdot \nabla) U_f \right] = \nabla \cdot \sigma_f \quad (2)$$

Where  $U_f$  is the velocity vector of fluid and  $\rho_f$  is the density of blood. The density of blood is equal to  $1060 \frac{kg}{m^3}$ . Also  $\sigma_f$  is the fluid stress tensor.

$$\sigma_f = -PI + \eta_f(\dot{\gamma}) \left[ \nabla U_f + (\nabla U_f)^T \right] \quad (3)$$

In relation (3),  $P$  is the blood pressure,  $I$  is the unit matrix,  $\eta_f(\dot{\gamma})$  is the blood viscosity and  $(\dot{\gamma})$  is the shear strain rate.

$$\dot{\gamma} = \sqrt{2 \operatorname{tra} \left[ \frac{1}{2} (\nabla U_f + (\nabla U_f)^T) \right]^2} \quad (4)$$

$$\frac{\eta_f(\dot{\gamma}) - \eta_{\infty,f}}{\eta_{0,f} - \eta_{\infty,f}} = \left[ 1 + (\lambda_f \dot{\gamma})^2 \right]^{\frac{(n-1)}{2}} \quad (5)$$

Where  $\eta_{0,f}$  and  $\eta_{\infty,f}$  are blood viscosities at zero and infinite strain rates, respectively. Also, the parameters  $n$  and  $\lambda_f$  are power index and stress relief time, respectively. The values of the parameters used are determined as follows:

$$\lambda_f = 3.313(s). \quad \eta_{0,f} = 0.056(Pa.s). \quad \eta_{\infty,f} = 0.00345(Pa.s). \quad n = 0.357 \quad (6)$$

To model the elastic artery in the isotropic state, Young's modulus with value  $E = 0.7$  MPa and Poisson's ratio with value  $\nu = 0.49$  have been used. The equation of motion of the elastic wall is written as follows:

$$\rho_s \frac{\partial^2 L_s}{\partial t^2} = \nabla \cdot \sigma_s \quad (7)$$

Where  $L_s$  are displacement vectors,  $\sigma_s$  are stress tensors in solids and  $\rho_s$  are elastic wall densities. The density of the elastic artery is  $\rho_s = 2000 \frac{kg}{m^3}$ . Assuming that the arterial wall is elastic, isotropic, and isothermal, Hooke's law is derived from the following relation:

$$\sigma'_s = 2 G_s \epsilon'_s \quad (8)$$

The parameters  $\sigma'_s$  and  $\epsilon'_s$  are the deflection stress tensor and the deflection strain tensor for the elastic wall, respectively, and are calculated as follows.

$$\sigma'_s = \sigma_s - \frac{1}{3} \operatorname{tra}(\sigma_s) I \quad (9)$$

$$\epsilon'_s = \epsilon_s - \frac{1}{3} \operatorname{tra}(\epsilon_s) I \quad (10)$$

Where  $I$  is a single matrix and  $\frac{1}{3} \operatorname{tra}(\sigma_s)$  is the mean stress at one point and  $\operatorname{tra}(\epsilon_s)$  is the strain change per unit volume. For the stress tensor equation, we have  $\sigma_s$ :

$$\sigma_s = 2G_s \epsilon_s - \Psi_s \operatorname{tra}(\epsilon_s) I \quad (11)$$

The parameters  $\Psi_s$  and  $G_s$  are the first and second lame parameters, respectively.

$$G_s = \frac{E}{2(1+\nu)} \quad (12)$$

$$\Psi_s = \frac{2G_s}{1-2\nu} \quad (13)$$

The governing equations at the common boundary of fluid and structure are defined as follows:

$$V_f(k.t) = V_s(k.t) \quad k \in \Gamma_{fs} \quad (14)$$

$$F_s(k.t) = F_f(k.t) \quad k \in \Gamma_{fs} \quad (15)$$

$\Gamma_{fs}$  Is the interface of the fluid and the structure and  $k$  is a point on the interface.

## IV. MESH INDEPENDENCE STUDY AND VALIDATION

In order to study the mesh independence, three different types of networking are used. The specifications of these networks are stated in Table (1).

Table 1. Number of elements used in three types of networking

N.O	Number of element
1	61313
2	79833
3	418663

To evaluate the mesh independence study, the size and velocity profile at different places and times for three types of networking have been compared and examined. Figure (2) shows the axial velocity for two different cross sections after the clogging area ( $Z' = 4/3, Z' = 2/5$ ) and at the time interval  $t/t_p = 0.75$ . The  $t_p$  parameter is the periodicity time and is equal to 0.345 seconds.  $Z'$  is also the axial distance from the center of the block, which is dimensionless with the size of the pipe diameter.

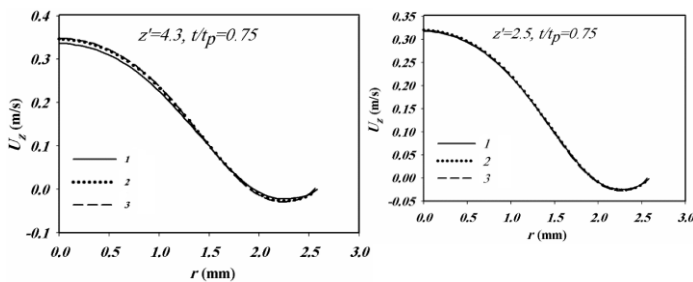


figure 2. Axial velocity profiles in two different cross sections after the clogging zone for two different times  
 According to Figure (2), the networking of the second case is independent of the solution and does not show much change as a result of reducing the mesh size.

In order to evaluate the accuracy and validity of the results of the present study, the flow of Newtonian fluid in the artery with an elastic wall was simulated and compared with the results of Lee and Xu [15]. A view of the eclipse geometry is shown in Figure (3).

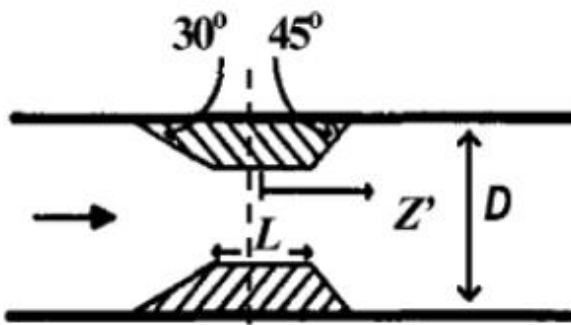


Figure 3. Schematic of geometry used by Lee and Xu[15]  
 The length of the blockage is 1.5 mm and the thickness of the vessel wall is 0.5 mm. The length of the artery before and after the blockage is 3 and 5 times the diameter of the artery, respectively. The current density is  $755 \frac{kg}{m^3}$  and the viscosity is  $0.00143 \frac{N.s}{m^2}$ .

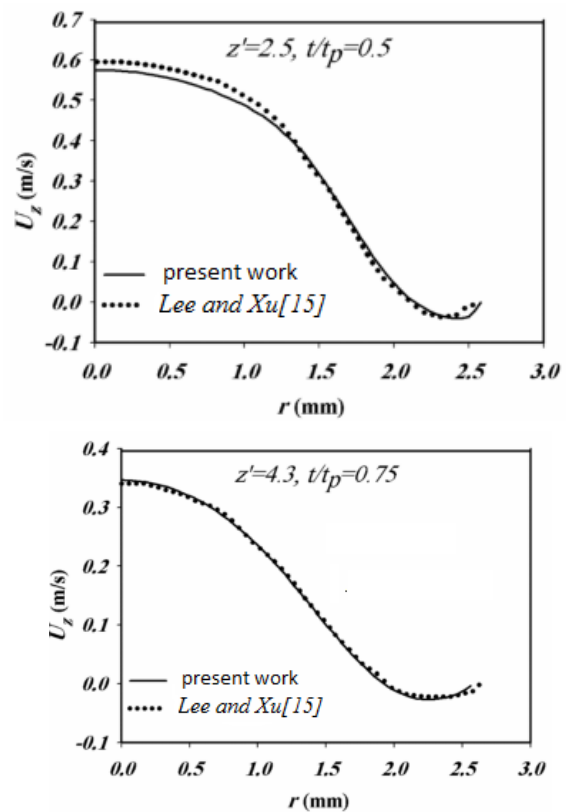


Figure 4. Comparison of the results of the present study with Lee and Xu [15]

## V. RESULTS AND DISCUSSION

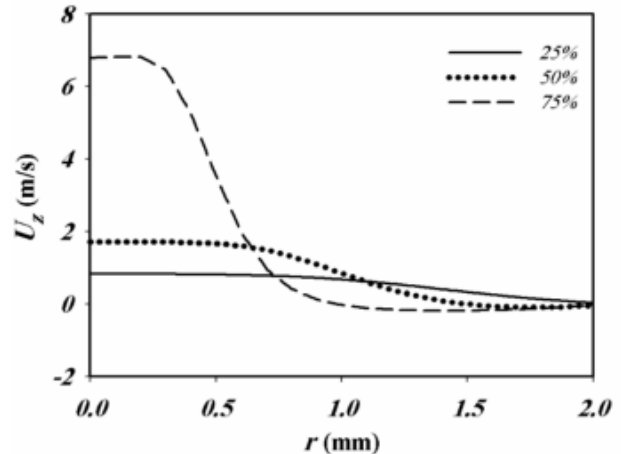


Figure 5. Intra-viscoelastic artery blood flow velocity profile for different percentage of clogs at peak flow time and at axial distance  $Z' = 2.5$

As the percentage of clogging increases, the cross-sectional area of the artery to pass blood flow decreases, which speeds up the flow. As the percentage of clogged arteries increases from 25% to 75%, the velocity increases 7.35 times and the slope of the profile changes 9.4 times.

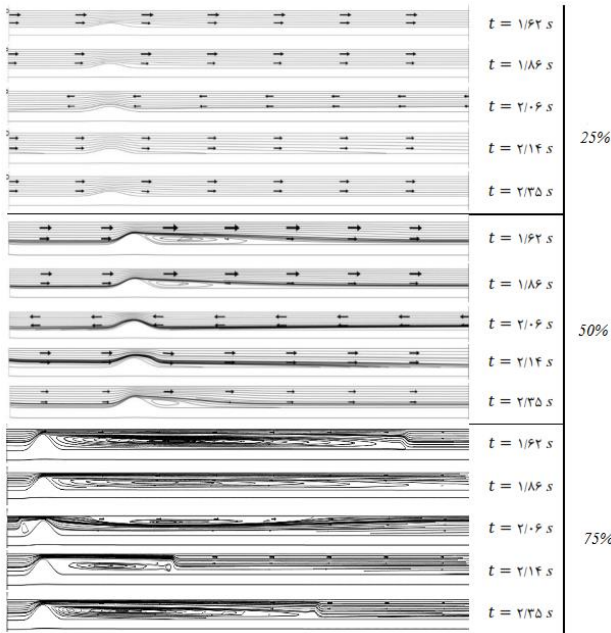


Figure 6. Impulsive flow lines of non-Newtonian fluid in the viscoelastic artery for different times at 25%, 50% and 75% clogs.

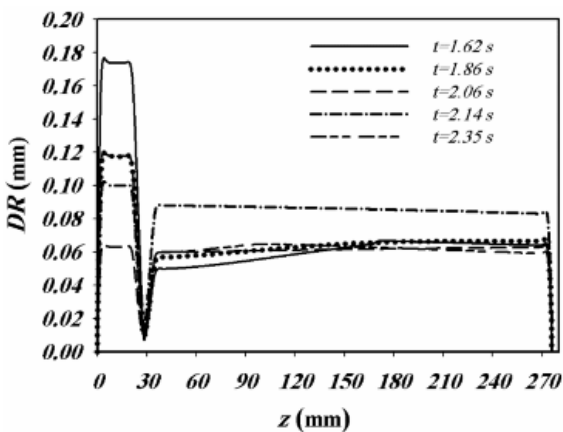


Figure 7. Radial displacement of the viscoelastic artery walls relative to the axial line for different times in 75% occlusion

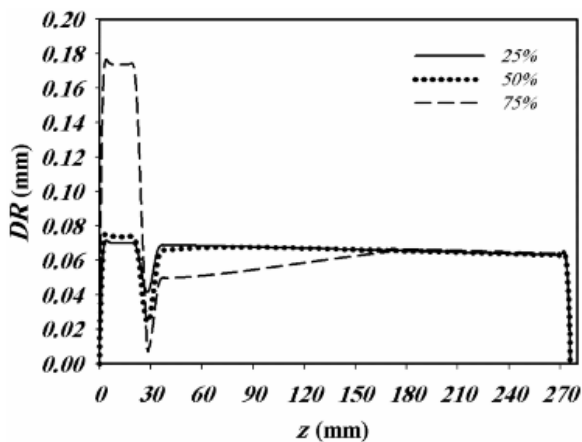


Figure 8. Radial displacement of the viscoelastic artery wall relative to the axial line for various types of clogging during peak flow

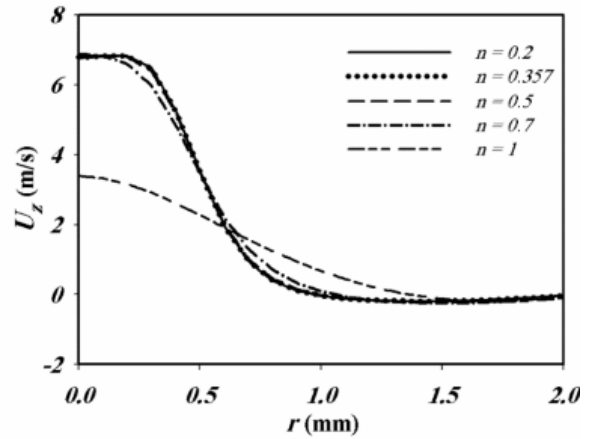


Figure 9. Intra-viscoelastic artery blood flow velocity profile for different values of power index with 75% clogging at distance  $Z' = 2.5$

Increasing the power index  $n$  leads to an increase in the viscosity of blood flow and this leads to a slowing down of blood flow inside the arteries.

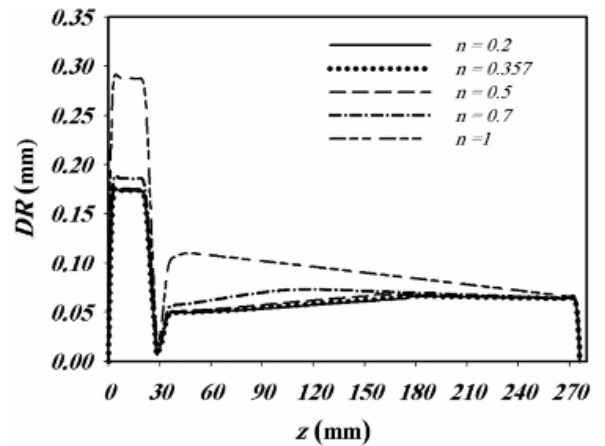


Figure 10. Radial displacement of arterial wall and viscoelastic relative to the axial line for different values of power index in 75% clogging

By increasing the power index  $n$  from 0.2 to 1, the radial displacement of the wall increases by 65.64%. The beginning and end of the artery have a displacement value of zero due to the constraint condition.

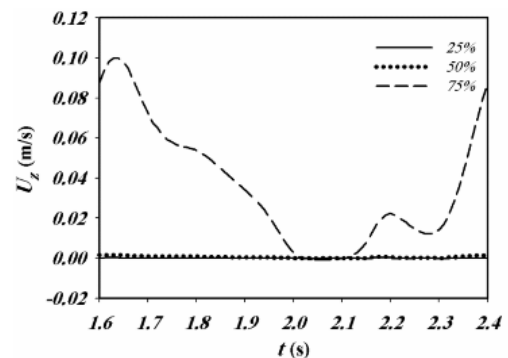


Figure 11. Changes in the axial velocity of the fluid at the boundary of the flow interaction with the wall of the viscoelastic artery occlusion region for different clogging percentages

For clogging intensity less than 50%, the velocity value is almost zero. But by increasing the clogging rate by 75%, it leads to an increase in speed by 612.87 times compared to 25% clogging.

## VI. Conclusion

- Increasing the percentage of clogged arteries leads to a 7.35-fold increase in velocity and a 9.4-fold increase in the slope of velocity profile changes after the clogging area.

- As the volumetric flow rate increases, the length of the vortex increases, and when the clogging intensity reaches 75%, the flow pattern becomes more complex.

- After the clogging zone, the radial displacement of the viscoelastic artery wall first has an upward trend (with a very gentle slope) and after the end of the vortex length, the trend of changes decreases with a gentle slope.

- Maximum shear stress occurs at the point of clogging and when the velocity size is at its maximum.

- By increasing the value of the power index from 0.2 to 1, the maximum shear stress of the wall at the clogging site increases by 8.62 times. Also, increasing the viscosity of blood flow leads to a 74.2% increase in blood pressure, a 65.64% increase in radial wall displacement and a 50.2% decrease in velocity before the occlusion area.

## REFERENCES

- [1] Boron W. F., E. L. Boulpaep, (2012), *Medical Physiology, 2e Updated Edition: with STUDENT CONSULT* Online Access: Elsevier Health Sciences,
- [2] Smith F., (1979). The separating flow through a severely constricted symmetric tube, *Journal of Fluid Mechanics*, Vol. 90, No. 04, pp. 725-754,
- [3] Deshpande M., D. Giddens, R. Mabon, (1976), Steady laminar flow through modelled vascular stenoses, *Journal of Biomechanics*, Vol. 9, No. 4, pp. 165- 174,
- [4] Young D. F., F. Y. Tsai, (1973), Flow characteristics in models of arterial stenoses—I. Steady flow, *Journal of biomechanics*, Vol. 6, No. 4, pp. 395-410,
- [5] Johnston B. M., P. R. Johnston, S. Corney, D. Kilpatrick, (2004), Non-Newtonian blood flow in human right coronary arteries: steady state simulations, *Journal of Biomechanics*, Vol. 37, No. 5, pp. 709-720,
- [6] Johnston B. M., P. R. Johnston, S. Corney, D. Kilpatrick, (2006), Non-Newtonian blood flow in human right coronary arteries: transient simulations, *Journal of Biomechanics*, Vol. 39, No. 6, pp. 1116-1128,
- [7] Buchanan Jr J., C. Kleinstreuer, J. Comer, (2000), Rheological effects on pulsatile hemodynamics in a stenosed tube, *Computers & Fluids*, Vol. 29, No. 6, pp. 695- 724,
- [8] Hussain A., (1986), Coherent structures and turbulence, *Journal of Fluid Mechanics*, Vol. 173, pp. 303-356,
- [9] Jung H., J. W. Choi, C. G. Park, (2004), Asymmetric flows of non-Newtonian fluids in symmetric stenosed artery, *Korea-Australia Rheology Journal*, Vol. 16, No. 2, pp. 101-108,
- [10] Perktold K., R. Peter, M. Resch, (1988), Pulsatile non-Newtonian blood flow simulation through a bifurcation with an aneurysm, *Biorheology*, Vol. 26, No. 6, pp. 1011-1030,
- [11] Hundertmark-Zaušková A., M. Lukáčová-Medvid'ová, G. Rusnáková, (2012), Fluid-structure interaction for shear-dependent non-Newtonian fluids, *Topics in mathematical modeling and analysis*, Vol. 7, pp. 109-158,
- [12] Chan W., Y. Ding, J. Tu, (2007), Modeling of non-Newtonian blood flow through a stenosed artery incorporating fluid-structure interaction, *ANZIAM Journal*, Vol. 47, pp. C507--C523,
- [13] Cho S. W., S. W. Kim, M. H. Sung, K. C. Ro, H. S. Ryou, (2011), Fluid-structure interaction analysis on the effects of vessel material properties on blood flow characteristics in stenosed arteries under axial rotation, *Korea-Australia Rheology Journal*, Vol. 23, No. 1, pp. 7-16,
- [14] Li M., J. Beech-Brandt, L. John, P. Hoskins, W. Easson, (2007), Numerical analysis of pulsatile blood flow and vessel wall mechanics in different degrees of stenoses, *Journal of Biomechanics*, Vol. 40, No. 16, pp. 3715-3724,
- [15] Lee K., X. Xu, (2002), Modelling of flow and wall behaviour in a mildly stenosed tube, *Medical engineering & physics*, Vol. 24, No. 9, pp. 575-586.